ACS Catalysis

Letter

pubs.acs.org/acscatalysis

Catalytic CO Oxidation over Well-Defined Cobalt Oxide Nanoparticles: Size-Reactivity Correlation

Viacheslav Iablokov,[†] Roland Barbosa,[†,‡] Glenn Pollefeyt,[§] Isabel Van Driessche,[§] Sergey Chenakin,[†] and Norbert Kruse*[,†,‡]

[†]Chemical Physics of Materials, Université Libre de Bruxelles, Campus Plaine, CP 243, Brussels B-1050, Belgium

[§]SCRiPTS, Department of Inorganic and Physical Chemistry, Ghent University, Krijgslaan 281-S3, 9000 Ghent, Belgium

[‡]Voiland School of Chemical Engineering and Bioengineering, Washington State University, Wegner Hall 155 A, Pullman, Washington 99164-6515, United States

Supporting Information

ABSTRACT: Co nanoparticles of well-defined size were synthesized by temperature-controlled injection of $Co_2(CO)_8$ into dichlorobenzene. After intercalation into mesoporous MCF-17 and temperature-programmed oxidation, Co_3O_4/MCF-17 model catalysts were obtained with cobalt oxide particle sizes varying between 3.5 and 12.2 nm. We demonstrate here the occurrence of a distinct particle size effect for the CO oxidation. Maximum reaction rates of about 0.77 nm^{-2} s^{-1} at 150 °C were observed for Co_3O_4 particles with a size in the range of 5 to 8 nm. The reaction rates decreased for either smaller or larger sizes. X-ray photoelectron spectroscopy allowed establishing a clear correlation between the Co^{3+} trivalent oxidation state and the CO oxidation rate.

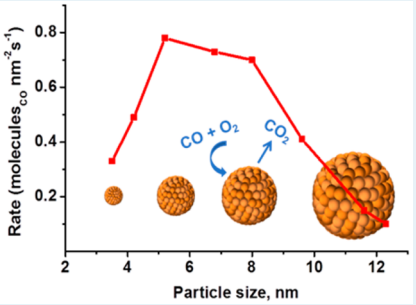

KEYWORDS: *particle size effect, cobalt nanoparticles, Co_3O_4 nanoparticles, catalytic CO oxidation, XPS*

The past decade has seen major efforts in making new concepts of nanotechnology available for catalyst preparation. Among these efforts, colloidal recipes turned out to be most versatile because they allow preparing nanosized metal particles while controlling their size and shape.[1] This, in turn, has sparked a number of investigations demonstrating that these geometrical parameters actually determine the catalytic activity and selectivity. The results are encouraging[2] and anticipate tunable catalyst properties for a variety of heterogeneous reactions.

One of the most striking examples of a metal particle size effect with regard to CO oxidation was discovered by Haruta et al.[3] Accordingly, nanosized gold particles supported on reducible oxides were found to be highly active in this reaction far below room temperature. More recently, the group of Somorjai,[4] in studies with Rh-based model catalysts, reported the shape of nanosized metal particles to play a decisive role in determining the selectivity of CO oxidation with NO. Another example is the unusual catalytic behavior of Ru nanoparticles (NPs).[5] Such Ru model catalysts showed the CO oxidation activity increased with size (i.e., 6 nm Ru NPs catalyst exhibited an 8-fold higher activity than 2 nm NPs).

While the strong influence of particle size and shape has been successfully demonstrated for metals, this is much less so for metal oxides. One of the reasons for this mismatch is the more complex crystal structure of metal oxides as compared to metals. As nanosized particles, these oxides may undergo structural modifications and adopt a variety of surface terminations with differing catalytic properties. For example, Co_3O_4 spinel, one of the most active oxides in the catalytic CO oxidation,[6] decomposition of N_2O,[7] or water splitting,[8] was reported to show morphology-dependent catalytic activity.[9] Co_3O_4 nanostructures with different shapes such as nanorods, nanobelts, nanocubes, and others were prepared to expose crystal planes with varying composition.[10] The (011) planes in these structures turned out to have the highest catalytic activity for CO oxidation and it was argued that, according to the atomic surface configuration, the (001) and (111) planes contain only Co^{2+}cations, whereas the (011) plane comprises mainly Co^{3+}cations. The abundance in Co^{3+} cations was related to superior CO oxidation activity; subsequently, these cations were claimed to be the active sites in CO as well as methane oxidation,[9,10] although no spectroscopic evidence was presented. Note that the size of the Co_3O_4 nanostructures in these studies was generally larger than 10 nm justifying morphology-dependent crystal plane variations rather than particle size effects to be responsible for alterations in the CO oxidation activity. Actually, to the best of our knowledge, no correlation between the particle size and catalytic activity, in particular for the CO oxidation over well-defined transition metal oxides, has ever been established before. The aim of this contribution was therefore to elucidate if a particle-size-derived structure−reactivity correlation is in operation for the CO oxidation reaction over a cobalt oxide catalyst.

Received: July 10, 2015
Revised: August 21, 2015
Published: August 25, 2015

DOI: 10.1021/acscatal.5b01452
ACS Catal. 2015, 5, 5714−5718

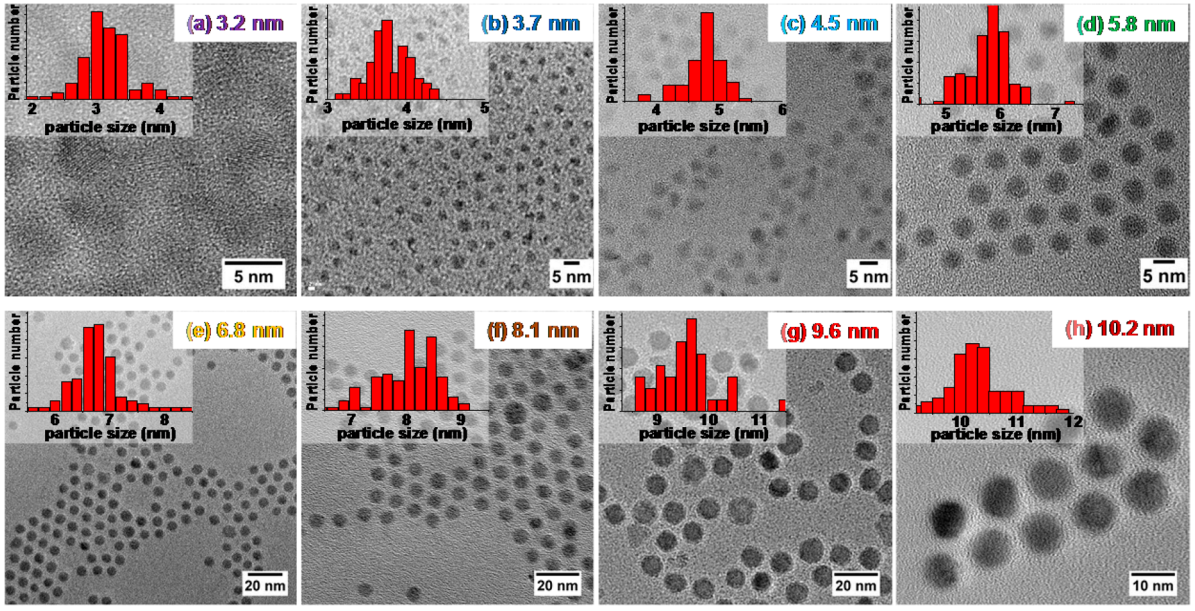

Figure 1. TEM images of Co NPs: (a) 3.2 nm, (b) 3.7 nm, (c) 4.5 nm, (d) 5.8 nm, (e) 6.8 nm, (f) 8.1 nm, (g) 9.6 nm, and (h) 10.2 nm.

Colloidal solutions of cobalt particles with well-defined size (standard deviation less than 8%) were prepared according to ref 11. Briefly, dicobaltoctacarbonyl precursor was injected into boiling dichlorobenzene solution containing oleic acid. Precise control of the reflux temperature while keeping constant the general conditions allowed preparing cobalt nanoparticles with well-defined sizes. Transmission electron microscopy (TEM) images of the colloidal Co NPs with sizes between 3.2 and 10.2 nm are shown in Figure 1. Subsequently, the cobalt nanoparticles (in dry chloroform) were impregnated into a meso-cellular foam (MCF-17) under sonication. TEM image of the impregnated 9.6 nm Co/MCF-17 sample is shown in Figure 2a. Due to the thickness of the MCF-17 structure, the cobalt particles could only be observed in the thinner periphery of the MCF-17 pore network.

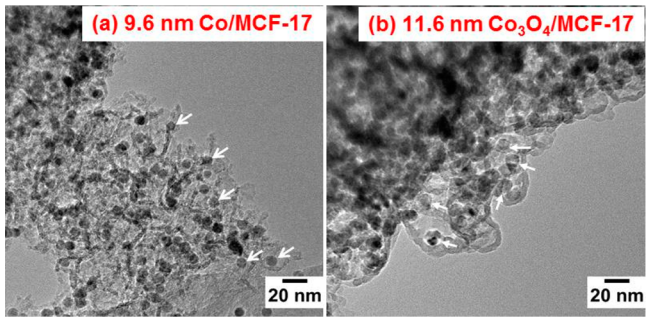

Figure 2. TEM images of (a) 9.6 nm Co/MCF-17 and (b) 11.6 nm Co_3O_4/MCF-17 sample obtained after TPO treatment of the 9.6 nm Co/MCF-17.

Next, the as-prepared Co/MCF-17 samples were subjected to temperature-programmed oxidation (TPO, 10% O_2 + Ar, see Figure S1) in order to transform Co metal into cobalt oxide. Clearly, the size of Co NPs is different from that of Co_3O_4 NPs due to the lattice expansion encountered during oxidation. We evaluated the size of Co_3O_4 NPs by using the bulk densities for metallic cobalt (8.90 g mL^{-1}) and cobalt oxide (6.11 g mL^{-1}). The obtained values are listed in Table S1. According to the TEM results, Co particles with a size of 9.6 nm were transformed into Co_3O_4 particles of about 11.6 nm while oxidizing Co/MCF-17 (Figure 2a,b). This is in good agreement with the calculated Co_3O_4 size (Table S1). Closer inspection of the crystal morphology seems to indicate the occurrence of common polyhedral shapes of cobalt oxide particles (see Figure S2). The observed shapes are thermodynamically favorable in the absence of strong support effects, which is the case for silica.

Co_3O_4/MCF-17 samples were tested for their CO oxidation activity without displacing them from the reactor after TPO. Because cobalt oxide NPs in distinct samples are "monodisperse" with a high degree of uniformity in size and shape, reaction rates in terms of "molecules (CO) nm^{-2} s^{-1}" (nm^{-2} s^{-1}) were calculated (see Supporting Information, section II). We refrain from calculating turnover rates in terms of converted CO molecules $site^{-1}$ s^{-1} since the exact nature of the catalytically active site in Co_3O_4 is considered unsettled for the time being.

The reaction rates in CO oxidation at 150 °C are plotted in Figure 3a as a function of the size of Co_3O_4 nanoparticles. Obviously, cobalt oxide particles with sizes between 5 and 8 nm exhibit the highest activity. The maximum reaction rate is about 0.77 CO molecules nm^{-2} s^{-1} at 150 °C (corresponding to 1.3 μmole CO m_{Co3O4}^{-2} s^{-1} for a size of 5.2 nm). The activity gradually decreases on either side of this size range.

Extrapolation to higher temperatures clearly demonstrates nearly identical activity as compared to noble metals (12−96 mL CO_2 m_{Me}^{-2} min^{-1} or 9−72 μmol CO m_{Me}^{-2} s^{-1} ranges for Pd or Rh particles deposited on γ-Al_2O_3 at 250 °C, and Pt at 300 °C).[12] The apparent activation energies of the CO oxidation over Co_3O_4/MCF-17 were obtained from Arrhenius plots in the temperature range of 140−200 °C, as shown in Figure 3b. The activation energies turned out to be very similar (i.e., independent of the Co_3O_4 particle size). Values between 70 and 75 kJ mol^{-1} were determined implying the same reaction mechanism should be in operation whatever the particle size. Most of the investigations up to date seem to favor a Mars−van Krevelen-type mechanism, which assumes surface

DOI: 10.1021/acscatal.5b01452
ACS Catal. 2015, 5, 5714−5718

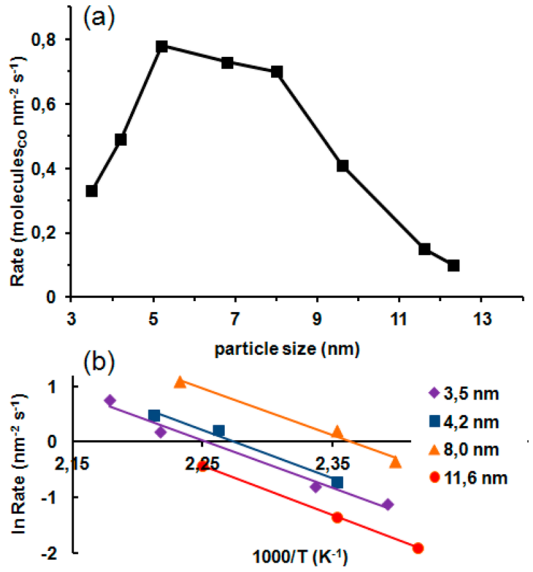

Figure 3. (a) CO oxidation activity (CO + O_2, 2% each, 150 °C) vs particle size, (b) Arrhenius plots for Co_3O_4/MCF-17 samples.

oxygen ions of the Co_3O_4 catalyst participate in the CO oxidation as part of an overall reduction−oxidation cycle.[13]

Literature reports on rate parameters for the CO oxidation over Co_3O_4 vary quite substantially. Somewhat larger or lower apparent activation energies (84 vs 60 kJ mol^{-1}) as compared to ours were obtained by Yu Yao[14] and Wang et al.,[6c] respectively. For similar reaction temperatures, their reaction rates in terms of μmol CO (or CO_2) g_{Co3O4}^{-1} s^{-1} were considerably smaller though. On the other hand, low-temperature measurements at approximately −80 °C by Haruta et al.[9,15] brought forth activation energies in the lower 20 kJ mol^{-1}, provided water inhibition effects were absent. Quite naturally, the reported reaction rates at this temperature were significantly lower than ours. The low activation energies[9,15] were explained by the facile formation of oxygen vacancies in the top surface layer. In the light of these results, it is surprising to note that the CO oxidation over Co_3O_4 type samples was classified "structure-insensitive".[6b]

Since the TEM results provided no indication for particle size-dependent 3D-morphological reshaping, electronic effects along with surface geometric rearrangements as a function of particle size have to be considered here. To obtain information on the valence state of the near-surface ions, we applied X-ray photoelectron spectroscopy (XPS). In these studies, Co NPs were deposited onto a gold foil and oxidized in a flow of 10% O_2 in Ar using the same TPO procedure and experimental conditions as applied when transforming Co/MCF-17 into Co_3O_4/MCF-17 for catalytic measurements. The occurrence of Co^{2+} and Co^{3+} species along with characteristic shakeup satellites in the Co 2p spectra of the TPO-treated NPs (Figure S3a) clearly demonstrated the formation of Co_3O_4 nanoparticles after TPO. The concomitant occurrence of CoO could be excluded from a close inspection of the satellite structure, which is known to be much more intense for Co^{2+} in CoO than for Co^{2+}/Co^{3+} in Co_3O_4.[16]

A detailed data analysis (all details on peaks assignment and deconvolution procedures are provided in the Supporting Information, section III) revealed specific trends in the species' core level and valence band photoemission with particle size. A most striking manifestation of a size effect is the strong variation in the shape of the O 1s core level peak. According to Figure 4a, the fractions of the components in the O 1s spectra which are attributed to O^{2-} lattice ions, hydroxyl groups (and/or chemisorbed O^- species) and adsorbed water, vary nonmonotonously with particle size so as to form extrema in the intermediate range between the smallest and largest particles size (Figure 4b). Interestingly, the O 1s fractional photoemission intensities of lattice O^{2-} and OH/O^- run counter each other and attain a maximum and minimum, respectively, at about 8 to 9 nm. Thus, a rather similar yet not identical dependence with NP size as that for the CO oxidation rates is obtained from the O 1s-derived spectral features (compare Figures 4b and 3a).

If turning to the valence band (VB)-derived Co 3d and O 2p contributions (Figure S5), further evidence for a distinct correlation between catalytic activity and surface electronic effects for varying particle sizes is obtained. In particular, the spectral weights (or fractions) of Co^{3+} 3d and O 2p are observed to vary significantly, in an opposite way and nonmonotonously with the Co_3O_4 NPs size, reaching a maximum and a minimum, respectively, at 5.2 nm (Figure 4c). The maximum Co^{3+} 3d intensity corresponds to a spectral weight of about 35% in the valence band for this particle size. We mention without showing that the width of the Co^{3+} 3d

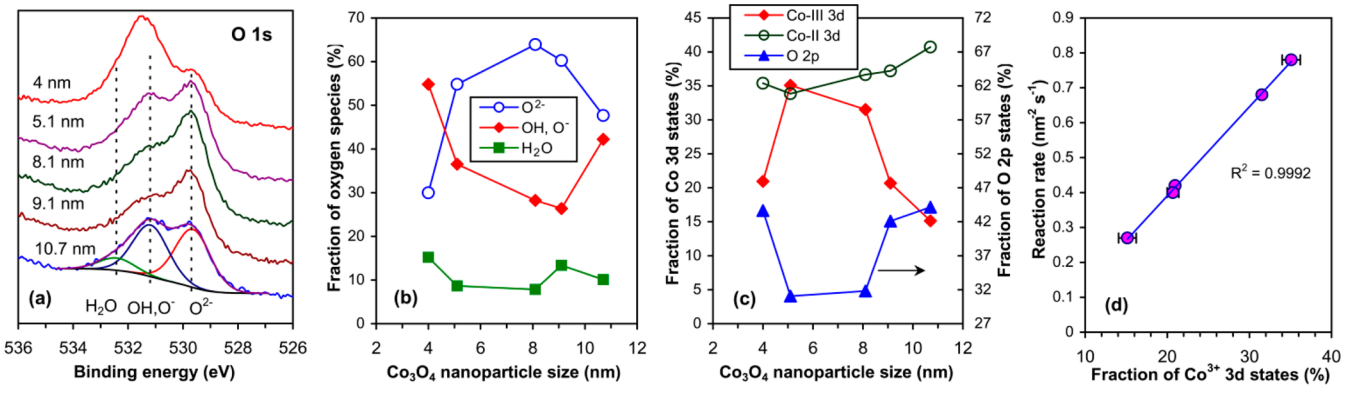

Figure 4. (a) XP O 1s spectra of cobalt oxide nanoparticles with varying size, (b) variation of the fractions of O^{2-}, OH (and/or O^-) and H_2O species derived from a deconvolution of the O 1s spectra as a function of Co NP size, (c) variation of spectral weights of the Co^{3+} 3d, Co^{2+} 3d and O 2p states in the valence band of cobalt oxide nanoparticles as a function of their size, and (d) correlation between the fraction of the Co^{3+} 3d states in the valence band of cobalt oxide NPs and reaction rate in catalytic CO oxidation over these particles at 150 °C.

DOI: 10.1021/acscatal.5b01452
ACS Catal. 2015, 5, 5714−5718

band also changes nonmonotonously attaining a maximum for the same particle size. The Co^{2+} 3d fractional intensity behaves very differently though. According to Figure 4c, this bivalent state species accumulates slightly and nonmonotonously over the range of investigated particle sizes. The similarity in the particle size dependence of the CO oxidation rate and the Co^{3+} 3d fractional intensity led us to plot Figure 4d from Figures 4c and 3a. Obviously, an excellent correlation is obtained demonstrating the importance of Co^{3+} (near-) surface amounts for this reaction. More precisely, the higher the density of the Co^{3+} 3d states in cobalt oxide nanoparticles, the higher is the CO oxidation rate. We note (data not shown) that also the $Co^{3+}3d/Co^{2+}3d$ and $Co^{3+}3d/O$ 2p fractional ratios produce an excellent correlation with the reaction rate.

It is interesting to note that no clear correlation with the catalytic activity seems to exist for the Co^{3+} 2p core level photoemission, notwithstanding the nonmonotonic variation of its fractional intensity with Co_3O_4 particle size (Figure S3 (b)). The discrepancy may be related to the higher sensitivity of the Co 2p states to specific chemisorption and surface rearrangement effects. Furthermore, while the O^{2-} component of the O 1s core level spectra in Figure 4b is clearly associated with the (near-surface) ionic structure of Co_3O_4, the OH/O^- component is certainly not. Instead, the latter component either arises from water (dissociative) adsorption or reflects charge compensation in relation with the polarity of the Co_3O_4 surface. The pronounced particle size dependence in Figure 4b seems to indicate the latter explanation applies here. Within the same line of thoughts, the VB-derived O 2p states would be largely influenced by surface effects.

To further deepen the understanding of our XPS results, it is useful to consider some of the results reported for the surface structure of oriented (111) and (011) Co_3O_4 films and particles.[17] Using low energy electron diffraction (LEED), scanning tunneling microscopy, and aberration-corrected TEM, these reports provide concurrent evidence for the polar surfaces of these morphological preparations to be (1 × 1) terminated. Quantitative LEED studies for (111) films—this orientation also dominates the slopes of our polyhedral nanoparticles—demonstrate a sublayer of cobalt ions in tetrahedral sites to terminate the surface. Interestingly, these cobalt ions seem to be in the trivalent rather than bivalent state as would be anticipated for bulk-terminated Co_3O_4 spinel. Actually, the charge redistribution mainly comprises the three outer layers, (Co^{2+} - O^{2-} - Co^{3+}), and as pointed out by R. Yu et al.,[17d] a dominant contribution to the compensation charges originates from the O^{2-} ions, in agreement with considerations of the electron polarization (which increases in the order Co^{3+} - Co^{2+} - O^{2-}). It is possible that the surface oxygen ions with reduced ionicity, as advocated by Yu et al.,[17d] contribute to the OH/O^- component of the O 1s core level envelope in our XP spectra.[16] Furthermore, the detailed LEED evidence presented in refs 17c,d demonstrates large relaxations to occur in the top layers of the (111) oriented films. Overall, strong modifications in the surface electronic density of states are produced this way and lead to charge compensation. It would appear that the details of this charge compensation and, consequently, the surface stability are dependent on the size of the nanoparticles in our measurements. Decreasing particle size will increase the number density of steps, so another level of complexity is introduced when it comes to optimizing the surface charges. Only when the Co_3O_4 particle sizes range between 5 and 8 nm will a relatively large 3d fractional contribution of trivalent Co^{3+} states along with a minimum of OH/O^- and O 2p derived states ensure high CO oxidation rates. Although the details of the charge compensation mechanisms with varying particle size must await further investigation, it may be safely assumed that the cobalt trivalent oxidation state plays a dominant role in providing the catalytically active sites for the CO oxidation over Co_3O_4.

To put our findings into a more general context, it appears Co_3O_4 is one of the most active metal oxides for CO oxidation. The reaction turns out to be structure-sensitive. This has been demonstrated here on the basis of a distinct particle size effect. The experimental approach included the synthesis of well-defined Co nanoparticles and, after intercalation into mesoporous MCF-17, temperature-programmed oxidation to Co_3O_4/MCF-17. Using X-ray photoelectron spectroscopy, we have been able to monitor the occurrence of surface compositional changes as a function of the size of Co_3O_4 nanoparticles. An excellent correlation between particles size and valence-band-derived Co^{3+} 3d states has been established, implying the importance of the trivalent state for attaining high reaction rates. A maximum rate has been found for particle sizes between 5 and 8 nm, which places such Co_3O_4 particles among the most active catalysts reported so far. Future work will address the very details of the particle size-dependent surface terminations using high-resolution aberration-corrected transmission electron microscopy.

■ ASSOCIATED CONTENT

Supporting Information

The Supporting Information is available free of charge on the ACS Publications website at DOI: 10.1021/acscatal.5b01452.

Experimental procedures, Figures S1−S5, and Table S1 (PDF)

■ AUTHOR INFORMATION

Corresponding Author

*E-mail: Norbert.Kruse@wsu.edu.

Notes

The authors declare no competing financial interest.

■ ACKNOWLEDGMENTS

R.B. acknowledges support by the Fond National de la Recherche Scientifique (FNRS) of Belgium. We thank Dr. Selim Alayoglu from the Lawrence Berkeley National Laboratory, US, for SEM characterization.

■ REFERENCES

(1) (a) Alivisatos, A. P. *Science* **1996**, *271*, 933−937. (b) Murray, C. B.; Kagan, C. R.; Bawendi, M. G. *Annu. Rev. Mater. Sci.* **2000**, *30*, 545−610. (c) Cushing, B. L.; Kolesnichenko, V. L.; O'Connor, C. J. *Chem. Rev.* **2004**, *104*, 3893−3946.

(2) (a) Somorjai, G. A.; Park, J. Y. *Angew. Chem., Int. Ed.* **2008**, *47*, 9212−9228. (b) Burda, C.; Chen, X.; Narayanan, R.; El-Sayed, M. A. *Chem. Rev.* **2005**, *105*, 1025−1102. (c) Fernandez-Garcia, M.; Martinez-Arias, A.; Hanson, J. C.; Rodriguez, J. A. *Chem. Rev.* **2004**, *104*, 4063−4104. (d) Zaera, F. *Chem. Soc. Rev.* **2013**, *42*, 2746−2762.

(3) Haruta, M.; Tsubota, S.; Kobayashi, T.; Kageyama, H.; Genet, M. J.; Delmon, B. *J. Catal.* **1993**, *144*, 175−192.

(4) (a) Dubois, L. H.; Hansma, P. K.; Somorjai, G. A. *J. Catal.* **1980**, *65*, 318−327. (b) Renzas, J. R.; Zhang, Y.; Huang, W.; Somorjai, G. A. *Catal. Lett.* **2009**, *132*, 317−322.

DOI: 10.1021/acscatal.5b01452
ACS Catal. 2015, 5, 5714−5718

(5) (a) Joo, S. H.; Park, J. Y.; Renzas, J. R.; Butcher, D. R.; Huang, W.; Somorjai, G. A. *Nano Lett.* **2010**, *10*, 2709−2713. (b) Kim, Y. D.; Over, H.; Krabbes, G.; Ertl, G. *Top. Catal.* **2000**, *14*, 95−100.
(6) (a) Jansson, J.; Palmqvist, A. E. C.; Fridell, E.; Skoglundh, M.; Osterlund, L.; Thormahlen, P.; Langer, V. *J. Catal.* **2002**, *211*, 387−397. (b) Royer, S.; Duprez, D. *ChemCatChem* **2011**, *3*, 24−65. (c) Wang, C.-B.; Tang, C.-W.; Gau, S.-J.; Chien, S.-H. *Catal. Lett.* **2005**, *101*, 59−63.
(7) Ohnishi, C.; Asano, K.; Iwamoto, S.; Chikama, K.; Inoue, M. *Catal. Today* **2007**, *120*, 145−150.
(8) Jiao, F.; Frei, H. *Angew. Chem.* **2009**, *121*, 1873−1876.
(9) (a) Xie, X.; Li, Y.; Liu, Z. Q.; Haruta, M.; Shen, W. *Nature* **2009**, *458*, 746−749. (b) Xie, X.; Shen, W. *Nanoscale* **2009**, *1*, 50−60.
(10) (a) Hu, L. H.; Sun, K. Q.; Peng, Q.; Xu, B. Q.; Li, Y. D. *Nano Res.* **2010**, *3*, 363−368. (b) Hu, L.; Peng, Q.; Li, Y. *J. Am. Chem. Soc.* **2008**, *130*, 16136−16137.
(11) Iablokov, V.; Beaumont, S. K.; Alayoglu, S.; Pushkarev, V. V.; Specht, C.; Gao, J.; Alivisatos, A. P.; Kruse, N.; Somorjai, G. A. *Nano Lett.* **2012**, *12*, 3091−3096.
(12) Yu Yao, Y.-F. *J. Catal.* **1984**, *87*, 152−162.
(13) Broqvist, P.; Panas, I.; Persson, H. *J. Catal.* **2002**, *210*, 198−206.
(14) Yu Yao, Y.-F. *J. Catal.* **1974**, *33*, 108−122. Yu, R.; Hu, L. H.; Cheng, Z. Y.; Li, Y. D.; Ye, H. Q.; Zhu, J. *Phys. Rev. Lett.* **2010**, *105*, 226101.
(15) Yu, Y.; Takei, T.; Ohashi, H.; He, H.; Zhang, X.; Haruta, M. *J. Catal.* **2009**, *267*, 121−128.
(16) Carson, G. A.; Nassir, M. H.; Langell, M. *J. Vac. Sci. Technol., A* **1996**, *14*, 1637−1642.
(17) (a) Vaz, C. A. F.; Wang, H.-Q.; Ahn, C. H.; Henrich, V. E.; Baykara, M. Z.; Schwendemann, T. C.; Pilet, N.; Albers, B. J.; Schwarz, U. D.; Zhang, L. H.; Zhu, Y.; Wang, J.; Altman, E. I. *Surf. Sci.* **2009**, *603*, 291−297. (b) Meyer, W.; Biedermann, K.; Gubo, M.; Hammer, L.; Heinz, K. *J. Phys.: Condens. Matter* **2008**, *20*, 265011. (c) Vaz, C. A. F.; Henrich, V. E.; Ahn, C. H.; Altman, E. I. *J. Cryst. Growth* **2009**, *311*, 2648−2654. (d) Yu, R.; Hu, L. H.; Cheng, Z. Y.; Li, Y. D.; Ye, H. Q.; Zhu, J. *Phys. Rev. Lett.* **2010**, *105*, 226101.

NOTE ADDED AFTER ASAP PUBLICATION

After this paper was published ASAP August 31, 2015, a correction was made to the description of Figure 2 in the first paragraph on page 5715. The corrected version was reposted September 4, 2015.

DOI: 10.1021/acscatal.5b01452
ACS Catal. 2015, 5, 5714−5718